Contribution from the Department of Chemistry,
Faculty of Science, Kyoto University, Sakyo-Ku, Kyoto 606, Japan

Metal-Thiolate Bonding Properties: Single-Crystal ESR, Susceptibility, and Polarized Absorption Evidence for a Strong π Interaction in Tetrakis(thiophenolato)cobaltate(II)

Kouichi Fukui, Norimichi Kojima, Hiroaki Ohya-Nishiguchi,* and Noboru Hirota

Received August 15, 1991

The single-crystal ESR, magnetic susceptibility, and polarized absorption results of $(Ph_4P)_2[Co^{II}(SPh)_4]$ are presented. This complex is known to possess a molecular geometry of approximate D_{2d} symmetry. From the single-crystal ESR results, the principal values of the apparent **g** tensor (**g'**) have been determined to be $g'_x < 0.6$, $g'_y < 1.5$, and $g'_z = 7.75 \pm 0.10$ with the molecular z axis coincident with the approximate D_{2d} geometry. The single-crystal susceptibilities in a temperature range of 1.6-100 K exhibit a remarkably large anisotropy indicative of a large zero-field splitting. Combination of the ESR and susceptibility results leads to the following estimate for the spin Hamiltonian parameters ($S = {}^3/_2$): $D = -70 \pm 10$ cm^{-1}, $|E/D| < 0.09$, $g_\perp = 2.2 \pm 0.1$, and $g_\parallel = 2.60 \pm 0.05$. The anomalous character of the complex, where the tetrahedral Co^{II} ion exhibits such a large zero-field splitting and a significant g anisotropy, should be noticed. The single-crystal polarized absorption results are analyzed with a view to characterizing the tetragonal ligand field. The one-electron d-orbital splitting thus obtained reveals a very large splitting between d_{z^2} and $d_{x^2-y^2}$ with d_{z^2} situated lower ($\mu = 4140$ cm^{-1}) and a rather small splitting between d_{xy} and $d_{yz,zx}$ with d_{xy} lower ($\delta = 1710$ cm^{-1}). This splitting pattern shows that a strong π interaction is incorporated in the cobalt(II)-thiolate bonding. This situation is described in a more quantitative fashion by use of the angular overlap model. The present findings are contrasted with the literature ones concerning iron(II)- and iron(III)-thiolate bondings.

Introduction

There are many metalloproteins which contain one or more cysteinyl thiolates coordinated to the active site metal ion(s). Typical examples of such metalloproteins are iron-sulfur proteins and blue-copper proteins.[1] In particular for blue-copper proteins, although they also contain other types of ligand coordination (two histidines and one methionine), their unusual spectroscopic properties have been attributed to some peculiarity in the Cu-SCys bonding.[2-5] It is therefore desirable to clarify the bonding properties between metal ions and thiolate sulfur atoms for better understanding of the electronic structure and, hopefully, the functional process of such thiolate-containing active sites. At present, however, only limited information is available about the metal-thiolate bonding properties despite many studies of model complexes and proteins.

Apart from the naturally expected large covalency, metal-thiolate bonding is marked by a significant influence of the thiolate S-C bond direction upon the overall electronic structure.[6-11] The S-C bond direction can be described in terms of two angles: the M-S-C angle and the X-M-S-C torsion angle, where X is another ligand atom. The M-S-C angle is typically 100-110°, and does not seem to vary from complex to complex. The X-M-S-C torsion angle, on the other hand, can vary if not sterically hindered and is relevant to the significant influence on the electronic structure. Then there are two possible explanations as to why variation of the torsion angle can affect the overall electronic structure: One is based on the nature of the metal-sulfur π interaction, where the sulfur π-bonding orbital is fixed perpendicular to the M-S-C plane.[12] The other is based on the nature of the metal-sulfur σ interaction. It is supposed that the sulfur σ-bonding orbital is directed away from the straight line toward the metal ion (misdirected valency).[13] However, it still remains controversial which explanation is in fact appropriate. Detailed spectroscopic studies on the active site of plastocyanin (one of the blue-copper proteins) by Solomon et al.[3-5] are indicative of strong π interaction between the copper ion and the cysteinyl sulfur atom, which accounts for the large intensity of the blue band. Ueyama et al.[7] have also stressed a role of the π interaction from model studies on rubredoxin (an iron-sulfur protein possessing the simplest $Fe(SCys)_4$ active site). However, recent studies on other rubredoxin models suggest that the π interaction is weak, and the concept of the misdirected valency explains rather well the spectroscopic properties of the model complexes.[8-10]

Here we describe the results of ESR, magnetic susceptibility, and polarized absorption measurements on single crystalline $(Ph_4P)_2[Co^{II}(SPh)_4]$. This complex has been already studied by X-ray crystallography, along with some analogues containing Fe^{II}, Zn^{II}, etc.[14] The X-ray studies show an approximate D_{2d} geometry for these complexes, where the S'-M-S-C torsion angles are all ca. 180°. This geometry can be compared with that of the rubredoxin active site.[15] Previously we have reported the polycrystalline ESR and magnetic susceptibility results of some co-

(1) (a) Adman, E. T. In *Metalloproteins, Topics in Molecular and Structural Biology*; Harrison, P. M., Ed.; Macmillan: New York, 1985; Vol. 6, pp 1-42. (b) Thomson, A. J. In ref 1a, pp 79-120; and references cited therein.
(2) (a) Ainscough, E. W.; Bingham, A. G.; Brodie, A. M.; Ellis, W. R.; Gray, H. B.; Loehr, T. M.; Plowman, J. E.; Norris, G. E.; Baker, E. N. *Biochemistry* **1987**, *26*, 71-82. (b) Brader, M. L.; Dunn, M. F. *J. Am. Chem. Soc.* **1990**, *112*, 4585-4587 and references cited therein.
(3) Penfield, K. W.; Gay, R. R.; Himmelwright, R. S.; Eickman, N. C.; Norris, V. A.; Freeman, H. C.; Solomon, E. I. *J. Am. Chem. Soc.* **1981**, *103*, 4382-4388.
(4) Penfield, K. W.; Gewirth, A. A.; Solomon, E. I. *J. Am. Chem. Soc.* **1985**, *107*, 4519-4529.
(5) Gewirth, A. A.; Solomon, E. I. *J. Am. Chem. Soc.* **1988**, *110*, 3811-3819.
(6) (a) Norman, J. G., Jr.; Jackels, S. C. *J. Am. Chem. Soc.* **1975**, *97*, 3833-3835. (b) Bair, R. A.; Goddard, W. A., III *Ibid.* **1978**, *100*, 5669-5676. (c) Noodleman, L.; Norman, J. G., Jr.; Osborne, J. H.; Aizman, A.; Case, D. A. *Ibid.* **1985**, *107*, 3418-3426.
(7) Ueyama, N.; Sugawara, T.; Tatsumi, K.; Nakamura, A. *Inorg. Chem.* **1987**, *26*, 1978-1981.
(8) Deaton, J. C.; Gebhard, M. S.; Koch, S. A.; Millar, M.; Solomon, E. I. *J. Am. Chem. Soc.* **1988**, *110*, 6241-6243.
(9) Gebhard, M. S.; Deaton, J. C.; Koch, S. A.; Millar, M.; Solomon, E. I. *J. Am. Chem. Soc.* **1990**, *112*, 2217-2231.
(10) Gebhard, M. S.; Koch, S. A.; Millar, M.; Devlin, F. J.; Stephan, P. J.; Solomon, E. I. *J. Am. Chem. Soc.* **1991**, *113*, 1640-1649.
(11) Fukui, K.; Ohya-Nishiguchi, H.; Hirota, N. *Bull. Chem. Soc. Jpn.* **1991**, *64*, 1205-1212.
(12) For arenethiolates, the orientation of the sulfur π-bonding orbital will be influenced by the dihedral angle between the M-S-C and the aromatic ring planes.[10] In $M(SPh)_4^{2-}$, however, the two planes are parallel, and thus the orientation of the π-bonding orbital does not alter.
(13) Liehr, A. D. *J. Phys. Chem.* **1964**, *68*, 665-722.
(14) (a) Swenson, D.; Baenziger, N. C.; Coucouvanis, D. *J. Am. Chem. Soc.* **1978**, *100*, 1932-1934. (b) Coucouvanis, D.; Swenson, D.; Baenziger, N. C.; Murphy, C.; Holah, D. G.; Sfarnas, N.; Simopoulos, A.; Kostikas, A. *J. Am. Chem. Soc.* **1981**, *103*, 3350-3362. Although important structural parameters of the Co^{II} complex are given in ref 14a, the atomic coordinates do not appear therein, nor are they available in the supplementary material. Hence we used the data of the isomorphous and isostructural Fe^{II} complex in ref 14b in order to know the orientations of the molecules in the unit cell.
(15) (a) Watenpaugh, K. D.; Sieker, L. C.; Jensen, L. H. *J. Mol. Biol.* **1979**, *131*, 509-522. (b) Frey, M.; Sieker, L.; Payan, F.; Haser, R.; Bruschi, M.; Pepe, G.; LeGall, J. *Ibid.* **1987**, *197*, 525-541. (c) Adman, E. T.; Sieker, L. C.; Jensen, L. H. *Ibid.* **1991**, *217*, 337-352.

0020-1669/92/1331-1338$03.00/0

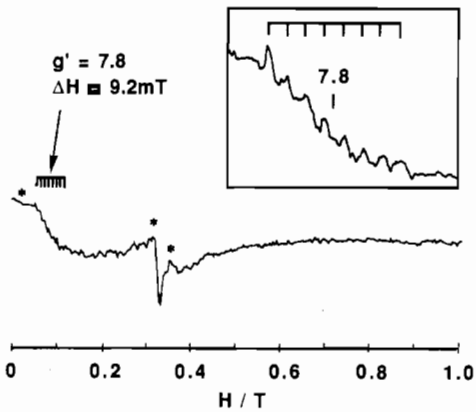

Figure 1. X-Band ESR spectrum of the Zn-doped polycrystalline powder of $(Ph_4P)_2[Zn(Co)(SPh)_4]$ (Co/Zn = 10%). Conditions: temperature, 4.2 K; sample amount, 30 μmol; power, 1 mW; amplitude, 1.25 × 1000; modulation, 10 G at 100 kHz. The signals marked with an asterisk are due to impurities. The $g' = 7.8$ signal is enlarged in the inset.

balt(II)–thiolate complexes including the title complex.[11] These results show that $(Ph_4P)_2[Co^{II}(SPh)_4]$ has anomalous magnetic properties, that is, a large zero-field splitting (ZFS) and highly anisotropic g values. We have suggested that these anomalous properties are related with its unique geometry of the D_{2d}-type thiolate coordination. In this paper, the origin of the anomalous properties is discussed in detail by means of the angular overlap model (AOM),[16,17] and is consequently attributed to the combination of the D_{2d} geometry and strong metal–sulfur π interaction. Comparison is also made between our results and the literature results for iron(II)– and iron(III)–thiolate complexes.[8-10,14,18]

Experimental Section

Material. $(Ph_4P)_2[Co^{II}(SPh)_4]$ and the analogous Zn^{II} complexes were prepared according to the reported method.[19] The Zn^{II} complex is isomorphous and isostructural with the Co^{II} complex (the orthorhombic space group $Pbc2_1$, $Z = 4$),[14] and was used as a host lattice for ESR and polarized absorption measurements. Neat single crystals of the Co^{II} complex were grown by slow evaporation (typically over a week) of acetonitrile solution at room temperature. Mixed single crystals were obtained in a similar manner from acetonitrile solution containing the Co^{II} and Zn^{II} complexes in a mole ratio of Co/Zn = 1% or 10%. The actual cobalt concentration in a Co/Zn = 10% mixed crystal was estimated to be Co/Zn = 12% from the solution-state absorbance at 416 nm ($\epsilon = 4380\ M^{-1}\ cm^{-1}$).[19] This suggests that no substantial change occurs in the Co/Zn ratio upon crystallization. The obtained crystals were in a form of rectangular prism with irregular-shaped edges. The long and short axes were found to be parallel to the crystal a and b axes, respectively, by using an X-ray diffractometer at the Institute for Molecular Science (Okazaki, Japan).

Measurements. ESR spectra were recorded on a JEOL FE-3X spectrometer equipped with an Air Products LTR-3-110 Heli-Tran liquid-helium-transferring refrigerator. The microwave frequency (X-band) was measured with a Takeda Riken TR5211 frequency counter. Cr^{III} in MgO ($g = 1.98$) was used as a calibrant of the magnetic field. Co/Zn = 10% mixed crystals were used for the measurements. They were mounted on a quartz rod, and rotated under a magnetic field with the field vector within either the ab, bc, or ac crystal plane. Because of the extremely weak nature of the ESR signal of the Co^{II} complex, we were forced to collect data near the detection limit of the apparatus. Hence, unfortunately, the obtained spectra were not free from impurity signals arising from somewhere in the apparatus, though these signals were easily distinguished by comparing the spectra with the null spectrum. (The impurity signals are marked with an asterisk in Figure 1.)

Magnetic susceptibility measurements were performed on a Faraday-type susceptometer by use of a neat crystal. Three cases ($H \| a$, $\| b$, and $\| c$) were examined over a temperature range of 1.6–100 K at a static magnetic field of 700 mT. Unfortunately the mass of the employed crystal (34 mg) was not sufficient for reliable measurements above 100 K. The magnetic field was measured with a Hall probe, and the temperature, with a thermocouple and a Ge resistor. The calibrations of the temperature and the field gradient were made using $KCr(SO_4)_2 \cdot 12H_2O$ and $HgCo(NCS)_4$, respectively.

Polarized absorption measurements were performed using a JASCO CT-100 spectrometer with a Glan–Taylor prism as a polarizer. The spectrometer was equipped with a HTV-R376 photomultiplier or a HTV-P819 PbS detector depending on whether the measurements concerned the visible region (12 000–18 000 cm^{-1}) or the near-infrared region (5000–12 000 cm^{-1}). Visible-region spectra were obtained with Co/Zn = 1% mixed crystals. As for near-infrared spectra, on the other hand, Co/Zn = 10% crystals were used to compensate for weaker absorption intensities in this region. Sliced crystals were irradiated with the electronic vector parallel to either the b or the c axis (the light propagation direction was always parallel to the a axis). Both regions were first examined at 77 K. However the visible-region spectra at 77 K were difficult to interpret owing to severe overlaping of absorption bands, which is not rare for high-spin tetrahedral Co^{II} complexes.[20] Thus the visible region was further examined at 4.2 K.

Analyses. The analysis of the single-crystal ESR data was made using the $S' = {}^1/_2$ effective spin Hamiltonian[21]

$$H = \sum_{p=x,y,z} \mu S'_p g'_p H_p + \mathbf{S'} \cdot \mathbf{A} \cdot \mathbf{I}$$

for the molecular-axis system or

$$H = \sum_{\alpha,\beta=a,b,c} \mu S'_\alpha g'_{\alpha\beta} H_\beta + \mathbf{S'} \cdot \mathbf{A} \cdot \mathbf{I}$$

for the crystal-axis system. Here $\mathbf{A}$ is the hyperfine coupling tensor due to ^{59}Co ($I = {}^7/_2$), and the other symbols have their usual meanings. Thus estimated g'_p values were interpreted in the framework of the $S = {}^3/_2$ spin Hamiltonian where the uniaxial $\mathbf{g}$ tensor is assumed as usual[22]

$$H = D(S_z^2 - {}^5/_4) + E(S_x^2 - S_y^2) + \mu g_\perp (S_x H_x + S_y H_y) + \mu g_\parallel S_z H_z$$

The single-crystal susceptibility data were analyzed using the $S = {}^3/_2$ spin Hamiltonian with $E = 0$ assumed additionally.

Ligand-field calculations were carried out at the Data Processing Center in Kyoto University. The excitation energies of d–d transition were computed by diagonalization of the electron–electron repulsion plus ligand-field matrix with the full basis set for the d^7 configuration employed.[23]

Results and Analyses

ESR Spectroscopy. We previously reported the polycrystalline ESR results for three forms of $(Ph_4P)_2[Co^{II}(SPh)_4]$: neat polycrystalline powder and two types of Zn-doped polycrystalline powder (Co/Zn = 10% and 1%).[11] Figure 1 shows the ESR spectrum of the Co/Zn = 10% powder, which exhibits only an extremely weak signal with an apparent g value of $g' = 7.8$ and a hyperfine splitting of 9.2 mT due to ^{59}Co ($I = {}^7/_2$). No other features assignable to this complex have been observed up to 1.0 T. The spectrum of the neat powder is practically identical with that of the Co/Zn = 10% powder, though the neat powder spectrum is much broader owing to larger dipolar interactions among the cobalt ions. From the Co/Zn = 1% powder, on the other hand, no signal could be observed. However this result is still consistent with the extremely weak intensities observed from the Co/Zn = 10% and the neat powders. Hence it is at least clear that the weakness of the ESR signal is not due to intermolecular exchange interaction. The ESR spectra, therefore, should be interpreted as originating from mononuclear Co^{II}. Accordingly we have concluded in the previous paper that the ZFS parameters of this complex are $D < 0$ and $E/D \approx 0$, and that the weak signal

(16) (a) Yamatera, H. *Bull. Chem. Soc. Jpn.* **1958**, *31*, 95–108. (b) Schäffer, C. E.; Jørgensen, C. K. *Mol. Phys.* **1965**, *9*, 401–412.
(17) Deeth, R. J.; Duer, M. J.; Gerloch, M. *Inorg. Chem.* **1987**, *26*, 2573–2578.
(18) (a) Phillips, W. D.; Poe, M.; Weiher, J. F.; McDonald, C. C.; Lovenberg, W. *Nature* **1970**, *227*, 574–576. (b) Eaton, W. A.; Lovenberg, W. In *Iron Sulfur Proteins*; Lovenberg, W., Ed.; Academic Press: New York, 1973; Vol. 2, Chapter 3.
(19) Dance, I. G. *J. Am. Chem. Soc.* **1979**, *101*, 6264–6273.
(20) (a) Ferguson, J. *J. Chem. Phys.* **1963**, *39*, 116–128. (b) Jesson, J. P. *Ibid.* **1968**, *48*, 161–168.
(21) Distinguish $\mathbf{g'}$ from $\mathbf{g}$: In this paper, $\mathbf{g}$ is specifically used for the $S = {}^3/_2$ spin Hamiltonian whereas $\mathbf{g'}$ is used for the $S' = {}^1/_2$ effective spin Hamiltonian. (In addition, the scalar parameter g' will be used to represent the ESR resonance position.) The relation between their principal values, namely g_p and g'_p, under the condition of ZFS ≫ Zeeman, is given elsewhere.[22]
(22) Drulis, H.; Dyrek, K.; Hoffmann, K. P.; Hoffmann, S. K.; Weselucha-Birczynska, A. *Inorg. Chem.* **1985**, *24*, 4009–4012.
(23) Griffith, J. S. In *The Theory of the Transition-Metal Ions*; Cambridge University: Cambridge, U.K., 1961.

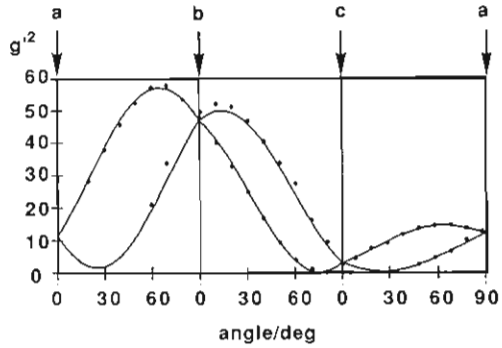

Figure 2. Angular variation of g'^2 from the single-crystal ESR data for $(Ph_4P)_2[Zn(Co)(SPh)_4]$ (Co/Zn = 10%) at 4.2 K. The solid curves represent least-squares fits.

Table I. Principal Values and Direction Cosines of the Apparent g Tensor of $(Ph_4P)_2[Co(SPh)_4]$ Determined from the Single-Crystal ESR Measurements

	direction cosines[a]		
g' values	*a*	*b*	*c*
$g'_x < 0.6$		*b*	
$g'_y < 1.5$		*b*	
$g'_z = 7.75 \pm 0.1$	0.415	−0.882	0.233
	−0.415	−0.882	0.233
	−0.415	0.882	0.233
	0.415	0.882	0.233

[a] Four sets appear for each component because of the presence of four molecules in the unit cell. [b] Could not be determined because the g' tensor is nearly uniaxial ($g'_x \approx g'_y$).

arises from the forbidden $-^3/_2 \rightarrow {}^3/_2$ transition. These conclusions are to be corroborated in this paper.

The single-crystal ESR spectroscopy will allow a definitive assignment of the sign of D and a more accurate estimate of E/D, providing further information about the principal g' values, of which only one component ($g' = 7.8$) was apparent in the polycrystalline spectra. Furthermore, the single-crystal spectroscopy can serve to determine the molecular-axis directions. In Figure 2, the angular variation of the observed signal positions are plotted as g'^2 vs θ. The appearance of two signals is consistent with the space group $Pbc2_1$ and $Z = 4$.[14] Under the space group the four molecules are divided into two sets of magnetically equivalent pairs when the magnetic field lies in a crystal plane. The signals were always weak analogous to the situation of the polycrystalline spectra. In particular, when the applied field was in the *ab* plane, the higher-field signal was too weak and broad to be detected. Thus, unfortunately, some of the data points corresponding to this signal are absent in Figure 2.

The hyperfine splitting due to ^{59}Co was observed at every angle of the three rotations. The coupling constant was found to be nearly isotropic as $|A| = (34 \pm 3) \times 10^{-3}$ cm^{-1}. This $|A|$ value is consistent with the hyperfine splitting observed in the powder spectrum, 9.2 mT for $g' = 7.8$.

From the $S' = {}^1/_2$ effective spin Hamiltonian, the following equation is obtained for the g' values under the magnetic field which is directed parallel to the crystal $\alpha\beta$ plane ($\alpha, \beta = a, b, c$) and forms an angle, e.g. θ, with the α axis:

$$g'^2 = (\sum_{\gamma=a,b,c} g'^2_{\alpha\gamma}) \cos^2\theta + (\sum_{\gamma=a,b,c} g'^2_{\gamma\beta}) \sin^2\theta \pm 2(\sum_{\gamma=a,b,c} g'_{\alpha\gamma} g'_{\gamma\beta}) \cos\theta \sin\theta \quad (1)$$

Here "±" in the third term is related with the presence of two magnetically nonequivalents in the unit cell. The components of the g' tensor were determined from the least-squares fit to this equation. The fits of the data are quite good as shown in Figure 2. Table I lists the resulting principal g' values and the direction cosines of the molecular z axes. Unfortunately the x- and y-axis directions could not be determined because the experiments could not clearly distinguish the g'_x and g'_y values; i.e., the g' tensor is uniaxial within experimental error. The relatively large uncertainties in g'_x and g'_y are due to both the absence of some data points for the *ab* plane rotation and the limit in attainable field strength in our apparatus (1.0 T). $g'_x < 0.6$ comes from the observation that the higher-field signal moved off over 1.0 T around $\theta = 80°$ of the *bc* plane rotation and around $\theta = 30°$ of the *ca* plane rotation.

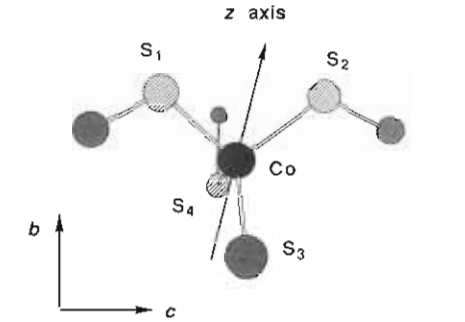

Figure 3. Direction of the molecular z axis with respect to the molecular frame of $Co(SPh)_4^{2-}$. A molecule in the unit cell and its z axis are viewed along the crystal c axis.

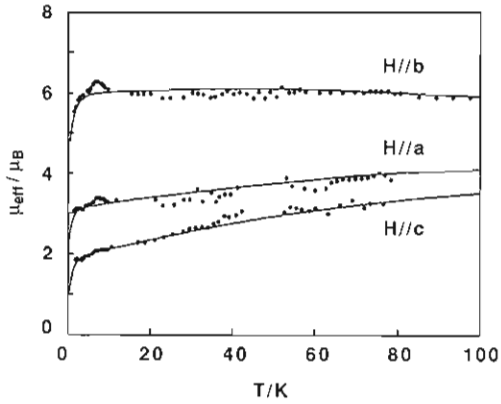

Figure 4. Temperature dependence of μ_{eff} from the single-crystal magnetic susceptibility data for $(Ph_4P)_2[Co(SPh)_4]$. The solid lines represent theoretical fits. The sudden drops around the low-temperature limit are due to saturation.

The $S = {}^3/_2$ spin system consists of two Kramers doublets, which are separated by $2(D^2 + 3E^2)^{1/2}$ ($=2D^*$) in the absence of a magnetic field. In the present complex this separation is very large (140 cm^{-1}) as will become clear from the susceptibility results (vide infra), so that the observed signals must correspond to the transition within the lower Kramers doublet. The $S = {}^3/_2$ spin Hamiltonian predicts that the principal g' values of the lower Kramers doublet are $2g_\perp$ and $g_\parallel$ for $D > 0$ and $E = 0$, and 0 ($=0g_\perp$) and $3g_\parallel$ for $D < 0$ and $E = 0$. Therefore we conclude $D < 0$, $E \approx 0$ (to be precise, the ratio E/D, not E itself, is nearly equal to zero), and $g_\parallel \approx g'_z/3 = 2.6$. The weak signals are thus undoubtedly ascribed to the forbidden $S_z = -^3/_2 \rightarrow {}^3/_2$ transition. The spin-Hamiltonian parameters can be estimated more definitively using eq 2 in ref 22, which includes the case for nonzero E. As a result, we estimate $|E/D| < 0.09$ and $g_\parallel = 2.60 \pm 0.05$, where $g_\perp = 2.2$ is used on the basis of the susceptibility results (vide infra).

In accordance with the four molecules in the unit cell, there are four possible sets of direction cosines for the z axis of a given molecule (Table I). Although purely experiment-based selection from the four possibilities is impossible, we can do this by referring to the molecular structure. The X-ray data[14] reveal that the present complex possesses an approximate D_{2d} geometry with the D_{2d} z axis bisecting the S_1–Co–S_2 and S_3–Co–S_4 angles (the literature numbering scheme is employed). Noticeably, one of the four possible z axes almost coincides with the D_{2d} z axis (Figure 3). This fact strongly suggests that the D_{2d} z axis is surely the actual z axis, and thus supports the D_{2d} approximation for this complex.

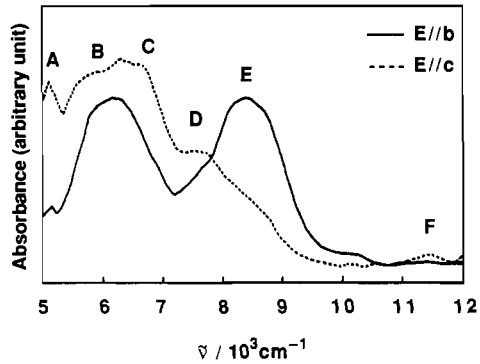

Figure 5. Single-crystal polarized absorption spectra of $(Ph_4P)_2[Zn(Co)(SPh)_4]$ (Co/Zn = 10%) for the near-infrared region at 77 K. The spectra for $E\|b$ and $E\|c$ are shown as a solid line and a dotted line, respectively.

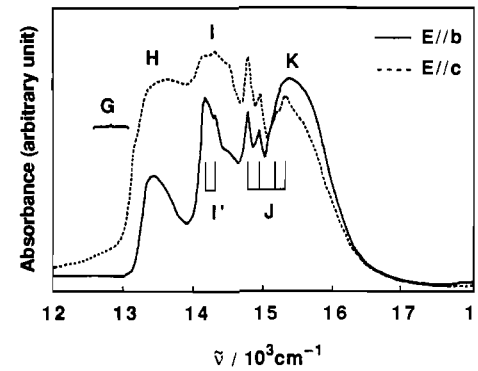

Figure 6. Single-crystal polarized absorption spectra of $(Ph_4P)_2[Zn(Co)(SPh)_4]$ (Co/Zn = 1%) for a visible region at 4.2 K. The spectra for $E\|b$ and $E\|c$ are shown as a solid line and a dotted line, respectively.

Magnetic Susceptibility. The single-crystal susceptibility data are plotted in Figure 4 as effective magnetic moment (μ_{eff}) vs T. The μ_{eff} values are significantly anisotropic even around 77 K. This is exclusively attributed to a large ZFS because the alternative explanation in terms of intermolecular interactions is ruled out by the variable cobalt-concentration ESR results[11] (vide supra). The increase of the anisotropy with decreasing temperature is thus attributed to thermal depopulation of the upper Kramers doublet. At extremely low temperatures, where only the lower doublet will be populated, μ_{eff} becomes 3.1 μ_B for $H\|a$, 6.0 μ_B for $H\|b$, and 1.9 μ_B for $H\|c$. (These are the values just before the sudden drop around the low-temperature limit, where saturation occurs.) It is important to note that these values are completely consistent with the ESR g' values. The μ_{eff} values at extremely low temperatures should be connected with the ESR g' values by $\mu_{eff} = (3/4)^{1/2}g'$. Thus, from the above μ_{eff} values, we have $g'^2(H\|a) = 13$, $g'^2(H\|b) = 48$, and $g'^2(H\|c) = 4.8$. These are in good agreement with the corresponding values of the ESR results (Figure 2), thereby demonstrating the complete consistency between the susceptibility and ESR results.

The variable-temperature susceptibility data are expected to provide complementary information concerning the spin-Hamiltonian parameters (D and $g_\perp$), which could not be determined by ESR spectroscopy. We have analyzed the susceptibility data in the framework of the $S = {}^3/_2$ spin Hamiltonian with an additional assumption of $E = 0$ for simplicity. This assumption is quite reasonable in view of the ESR results and can greatly simplify the situation in that we need not concern ourselves with the directions of the x and y axes. It is also important to note that the four molecules in the unit cell become magnetically equivalent under the experimental condition that the magnetic field is parallel to one of the crystal axes. This allows an unambiguous analysis of the susceptibility data. The best fit has been achieved using $D = -70 \pm 10$ cm^{-1}, $g_\perp = 2.2 \pm 0.1$, $g_\| = 2.7 \pm 0.1$, $|l_z| = 0.44$, $|m_z| = 0.86$, and $|n_z| = 0.26$, where l_z, m_z, and n_z are the direction cosines of the z axis. The resulting sign of D, the direction cosines, and the $g_\|$ value are, of course, in good agreement with those from the ESR results.

Polarized Absorption Spectroscopy. The spectra for the near-infrared region (5000–12 000 cm^{-1}) and for the visible region (12 000–18 000 cm^{-1}) are shown in Figures 5 and 6, respectively. The trend of the spectra well agrees with that of the solid-state reflectance spectrum, where the absorption maxima appear at 6009, 8333 (sh), and 13 888 cm^{-1}.[14] As for the solution-state spectrum, the absorption maxima appear at 6900 (broad), 13 800, 14 700, and 16 000 cm^{-1}.[14,19] Since it is not clear whether the geometric distortion around Co^{II} remains identical in the solution state, the fine structure in Figure 6 does not necessarily accord with that of the solution-state spectrum. However, the ligand-field parameters ($B \approx 640$, $Dq \approx -400$ cm^{-1}) estimated from the solution-state spectrum will be helpful later in ligand-field calculations.

Twelve absorption bands are resolved in Figures 5 and 6. We label them from A to K and collect their peak positions and polarization properties in Table II. A brief comment is necessary: Band C may be a part of band B. However, we treated them as separate bands because the absorbances at 6600 and around 6000 cm^{-1} in the b spectrum are substantially different. In the region 14 000–14 700 cm^{-1}, there appear to be two overlapping bands with different polarization properties. We labeled the broader one as band I and the sharper one as band I'. Band I' exhibits a structure probably due to vibronic coupling. Band J also exhibits a structure extending onto the region of band K. Both bands I' and J are attributable to spin-forbidden transitions borrowing intensities from their adjacent spin-allowed transitions.

Table II. Results from the Single-Crystal Absorption Measurements on $(Ph_4P)_2[Co(SPh)_4]$

label	ν/cm^{-1}	polarization	comment
A	5130	c	sharp
B	5800	c > b	broad
	6300	c > b	broad
C	6600	c > b	shoulder
D	7600	c	
E	8400	b	
F	11400	c	weak
G	12700	c	shoulder
	13170	c	edge-like shoulder
H	13400	c ≫ b	
I	14300	c ≫ b	broad
I'	14200	b[a]	sharp
	14320	b[a]	sharp
J	14787	b ≈ c	sharp
	14948	b ≈ c	sharp
	15170	c[b]	
	15310	c[b]	
K	15350	b > c	

[a] Merged in band I in the c spectrum. [b] Merged in band K in the b spectrum.

For tetrahedral high-spin Co(II) complexes, there are three spin-allowed ligand-field transitions; ${}^4A_2 \rightarrow {}^4T_2$, a^4T_1, and b^4T_1. For the present complex, they are expected to appear around 4000, 7000, and 14 500 cm^{-1}, respectively, from the solution-state spectrum.[14,19] These excited states are split under the D_{2d} ligand field into sublevels termed as ${}^4T_2;x,y$ and $(a,b)^4T_1;x,y$ (${}^4E$ under D_{2d}), ${}^4T_2;z$ (${}^4B_2$ under D_{2d}), and $(a,b)^4T_1;z$ (${}^4A_2$ under D_{2d}). Here the neglect of spin–orbit interactions is appropriate because the alternating behavior of the absorbances indicates that noncubic ligand fields are crucial to the splittings. The selection rules under D_{2d} symmetry are that ${}^4A_2 \rightarrow {}^4\Gamma;x,y$ ($\Gamma = T_1, T_2$) is allowed under x,y polarization, and ${}^4A_2 \rightarrow {}^4\Gamma;z$ ($\Gamma = T_1$) is allowed under z polarization while ${}^4A_2 \rightarrow {}^4T_2;z$ is still electric-dipole forbidden. The ${}^4\Gamma;x,y$ states will be further split owing to lower-symmetry fields. Then the x,y-polarized transition will be split correspondingly into two separate transitions, i.e., x- and y-polarized transitions when the x and y axes are chosen suitably.

Since the molecular z axis is almost perpendicular to the c axis as determined by ESR spectroscopy (Figure 3), the z-polarized

transitions should exhibit greater absorption in the $E\|b$ spectrum than in the $E\|c$ spectrum while the x,y-polarized transitions should exhibit greater absorption in the $E\|c$ spectrum.[24] Inspection of the observed spectra suggests that the nondegenerate x- and y-polarized transitions exhibit a polarization pattern similar to that of the degenerate x,y-polarized transitions: Note that there are only two bands (bands E and K) exhibiting more intensity in the $E\|b$ spectra, and the number 2 matches with the expected number of z-polarized transitions. Additionally, the strongest candidate for the x and y axes are the bisectors of the S_1–Co–S_3 and S_2–Co–S_3 angles.[25] Their direction cosines are ($|l|$, $|m|$, $|n|$) = (0.788, 0.261, 0.558) and (0.471, 0.328, 0.819), respectively,[14] suggesting again a polarization pattern of $E\|b < E\|c$ for the nondegenerate x- and y-polarized transitions.

On the basis of the above consideration, the band assignments are made as follows. There are only two bands (bands E and K) that become more intense under $E\|b$ than under $E\|c$. Hence it is straightforward to assign bands E and K to $^4A_2 \rightarrow a^4T_1;z$ and $^4A_2 \rightarrow b^4T_1;z$, respectively. Other prominent bands (bands H and I) in the visible region are therefore assigned to $^4A_2 \rightarrow b^4T_1;x,y$. Bands F, G, I′, and J are attributed to some spin-forbidden transitions. The assignment for $^4A_2 \rightarrow a^4T_1;x,y$ is less straightforward. However it seems unambiguous that band D corresponds to a component of $^4A_2 \rightarrow a^4T_1;x,y$. The partner of band D is probably band C. The remaining dipole-allowed transition is $^4A_2 \rightarrow {}^4T_2;x,y$, and hence band A is assigned to a component of this transition with its partner presumedly below 5000 cm^{-1}. The last band (band B), however, is difficult to be assigned because this band is equally intense under $E\|b$ and $E\|c$, and no such transitions are normally expected. We tentatively assign band B to a vibronic sideband of band A.

Discussion

The single-crystal ESR and susceptibility results clearly show that this complex possesses significantly anisotropic g values ($g_\perp$ = 2.2, $g_\parallel$ = 2.60), and an unusually large ZFS with negative D (=–70 cm^{-1})[26] and small rhombicity ($|E/D| < 0.09$). This situation is completely consistent with our previous conclusions drawn from the polycrystalline ESR and susceptibility results,[11] except that the D and $g_\parallel$ values were overestimated in the previous study.[27]

It also become clear that the ESR signal arises from the forbidden $S_z = -^3/_2 \rightarrow {}^3/_2$ transition, and this is the reason for the extremely weak intensity of the signal. It might seem strange that the allowed $-^1/_2 \rightarrow {}^1/_2$ transition within the upper doublet was not observed. The reason is 2-fold: (1) Because of the large ZFS in this complex, the thermal population of the upper doublet is not sufficient around 4.2 K. (2) At higher temperatures, on the other hand, the fast spin-relaxation phenomenon characteristic of high-spin Co^{II} complexes prevents any transitions from being detected. Actually, the signals described so far could not be observed above 10 K. Therefore it seems impossible to detect the transition within the upper doublet.

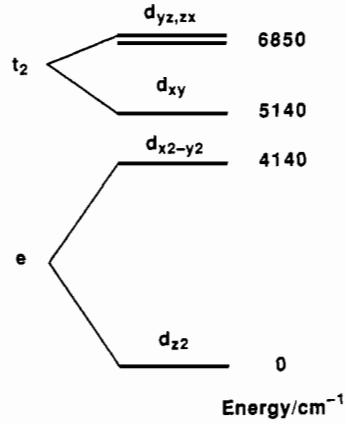

Figure 7. d-Orbital splitting scheme for $(Ph_4P)_2[Co(SPh)_4]$. For the ligand-field parameters, see the text or footnote *b* in Table III.

Table III. Observed and Calculated Excitation Energies of the Quartet States in $(Ph_4P)_2[Co(SPh)_4]$

level term	energy/cm^{-1} obsd[a]	energy/cm^{-1} calcd[b]
$^4A_2$	ground state	0
$^4T_2;z$	~1000[c]	1000
$^4T_2;x,y$	<5000, 5130 (~5000)	4850
$a^4T_1;x,y$	6600, 7600 (7100)	7360
$a^4T_1;z$	8400	8200
$b^4T_1;x,y$	13400, 14300 (13850)	14000
$b^4T_1;z$	15350	15300

[a] The values in the parentheses are the barycenters of the x and y components. [b] Obtained using Dq = –421 cm^{-1}, μ = 4140 cm^{-1}, δ = 1710 cm^{-1}, and B = 590 cm^{-1}. [c] Estimated from the D and $g_\parallel$ values.

The $g_\parallel$ and D values are indicative of an significant lowering of the $^4T_2;z$ level. Although the transition to this level were not observed in the polarized absorption spectra, its transition energy can be estimated from the $g_\parallel$ and D values. $g_\parallel$ and D are connected with the transition energies of $^4A_2 \rightarrow {}^4T_2;z$ and $\rightarrow {}^4T_2;x,y$ (denoted by Δ_z and $\Delta_{x,y}$, respectively) as[23]

$$g_\parallel = 2 - 8k\lambda/\Delta_z \quad (2a)$$

$$D = 4\lambda^2(1/\Delta_{x,y} - 1/\Delta_z) \quad (2b)$$

Here k and λ have their usual meanings, and we take $\lambda = k\lambda_{free}$ (λ_{free} = –178 cm^{-1}). Using k = 0.7,[11] we calculate Δ_z = 1160 cm^{-1} from eq 2a. Equation 2b gives a similar value of Δ_z = 750 cm^{-1}, where $\Delta_{x,y}$ = 5000 cm^{-1} is used according to the polarized spectral results. (Variation of $\Delta_{x,y}$ around this value does not alter appreciably the resulting Δ_z value.) Both estimates clearly show that the separation between $^4A_2$ and $^4T_2;z$ is only around 1000 cm^{-1}. The very slight disagreement between the two estimates may be due to the neglect of the contribution of doublet states to D. The information that $\Delta_z \approx 1000$ cm^{-1} greatly serves the following ligand-field calculations because the separation between $^4A_2$ and $^4T_2;z$ is equal to the separation between $d_{x^2-y^2}$ and d_{xy} in the one-electron scheme.

Now that all of the spin-allowed ligand-field transition energies are known, it becomes practical to determine the one-electron ligand-field splitting. The one-electron ligand-field splitting under D_{2d} symmetry is described in terms of three parameters, $10Dq$, μ, and δ:[23] $10Dq$ is the separation between the centers of the e and t_2 orbitals and is negative in tetrahedral complexes. μ is the separation between d_{z^2} and $d_{x^2-y^2}$ and is positive when d_{z^2} is lower. δ is the separation between d_{xy} and $d_{yz,zx}$ and is positive when d_{xy} is lower. On the basis of the information that the separation between $d_{x^2-y^2}$ and d_{xy} is around 1000 cm^{-1}, we reduced the number of the parameters by setting $\delta = -15Dq - (3/4)\mu - (3/2)\Delta_z$ and Δ_z = 1000 cm^{-1}.[28]

(24) For ideal x,y- and z-polarized transitions, the ratios of the absorbance in the $E\|b$ spectrum to that in the $E\|c$ spectrum (polarization ratio) should be 0.23 and 14.3, respectively, as estimated from the z-axis direction cosines listed in Table I. For details of the polarization ratio, see: Makinen, M. W.; Hill, S. C.; Zeppezauer, M.; Little, C. L.; Burdett, J. K. *J. Am. Chem. Soc.* **1987**, *109*, 4072–4081 and references cited therein.

(25) Winkler, H.; Bill, E.; Trautwein, A. X.; Kostikas, A.; Simopoulos, A.; Terzis, A. *J. Chem. Phys.* **1988**, *89*, 732–740.

(26) It may be worth mentioning that D = –70 cm^{-1} is unusual, but still concurrent with the criterion proposed by Makinen et al.: Makinen, M. W.; Kuo, L. C.; Yim, M. B.; Wells, G. B.; Fukuyama, J. M.; Kim, J. E. *J. Am. Chem. Soc.* **1985**, *107*, 5245–5255.

(27) In the previous paper we estimated D = –100 cm^{-1}, $g_\perp$ = 2.25, and $g_\parallel$ = 3.13. This overestimate comes from the fact that the observed powder susceptibilities were invariably larger than the spatial averages of the single-crystal susceptibilities. Such an upward shift of powder susceptibilities was also reported in the literature. This phenomenon was attributed to field-induced alignment of microcrystals in the powder sample. See: (a) Kennedy, B. J.; Murray, K. S. *Inorg. Chem.* **1985**, *24*, 1552–1557. (b) Boinnard, D.; Cassoux, P.; Petrouleas, V.; Savariault, J.-M.; Tuchagues, J.-P. *Inorg. Chem.* **1990**, *29*, 4114–4122.

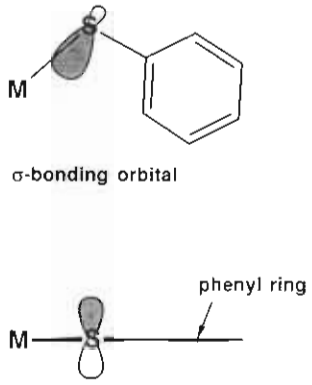

Figure 8. Two thiolate sulfur orbitals relevant to metal–thiolate bonding. The σ-bonding orbital may be misdirected within the M–S–C plane, and the π-bonding orbital is perpendicular to this plane (and also to the phenyl-ring plane).

In seeking for the best-fit values of the ligand-field parameters and the Racah parameter B, we first fixed Dq and B at the values estimated from the solution-state spectrum: $B \approx 640$ cm^{-1}, and $Dq \approx -400$ cm^{-1}. This leaves only one free parameter, μ. We performed the ligand-field calculations for various μ values, and found that good agreement with the experimental energies occurs only when μ is positive and large. The most suitable value is $\mu = 4500$ cm^{-1} (this gives $\delta = 1125$ cm^{-1}). It is therefore clear that, in the present complex, the e orbital split largely with d_{z^2} lower while the t_2 orbital split modestly with d_{xy} lower. Having known the approximate values for the parameters, we subsequently allowed all the parameters (except Δ_z[28]) to vary. The finally obtained best-fit values are $B = 590$, $Dq = -421$ cm^{-1} $\mu = 4140$ cm^{-1} and $\delta = 1710$ cm^{-1}. The one-electron ligand-field splitting thus determined is shown in Figure 7, and the calculated transition energies are compared with the experimental ones in Table III.

We have attributed bands F, G, I′, and J to unspecified spin-forbidden transitions. The ligand-field calculation may give further assignments of these bands. Accordingly we attempted to compute the excitation energies of the spin-forbidden transitions in the framework of the usual ligand-field theory. Use of the above parameter values and the ratio for the Racah parameter ($C/B = 4.63$) yields 11 770–11 930 (a^2T_1 and a^2E), 12 830 ($a^2T_2;z$), 13 060 ($^2A_1$), 14 770 ($b^2T_1;z$), and 15 740 cm^{-1} ($a^2T_2;x,y$), etc. On the basis of these results, we assign band F to the almost degenerate $^4A_2(S_z = \pm^3/_2) \rightarrow a^2T_1$, a^2E transitions.[29] Band G is also assigned reasonably to $^4A_2 \rightarrow {}^2A_1$, $a^2T_2;z$. For these bands, the observed polarization properties agree with the expected ones.[29] Although the transition $^4A_2 \rightarrow a^2T_1;x,y$ is expected to be z polarized, this transition should be weaker than its x,y-polarized partner $^4A_2 \rightarrow a^2T_1;z$ because of the longer distance to $^4A_2 \rightarrow b^4T_1;z$, from which $^4A_2 \rightarrow a^2T_1;x,y$ borrows intensity. As for the other hands, bands I′ and J may be assigned to $^4A_2 \rightarrow b^2T_1;z$ and $^4A_2 \rightarrow a^2T_2;x,y$, respectively, from the calculated energies. However, the observed polarization properties do not agree with the expected ones. At the moment, it is not known whether these bands should be assigned otherwise or if the disagreement is a result of too strong an interaction with $^4A_2 \rightarrow b^4T_1$.

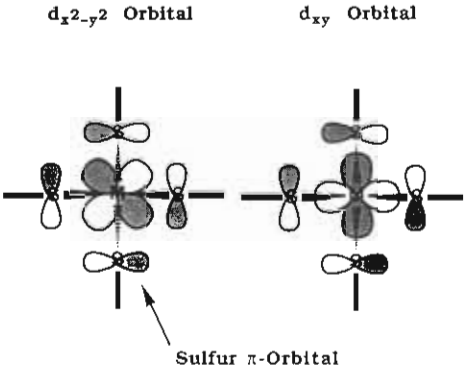

Figure 9. Effects of sulfur π-bonding orbitals under the D_{2d} geometry. The sulfur π orbitals interact mostly with $d_{x^2-y^2}$ whereas no interaction occurs with d_{xy}.

Thiolates can form two types of bonding with a metal ion; σ bonding and π bonding (Figure 8). The π-bonding orbital is directed perpendicular to the M–S–C_α plane. The σ-bonding orbital, on the other hand, may be misdirected within the M–S–C_α plane because of the orthogonality among the sulfur 3p orbitals.[9,10] The one-electron ligand-field splitting determined above can be used to probe how the two types of bonding influence the electronic structure of the complex. For this purpose the AOM is useful.[30]

The AOM one-electron d-orbital energies under D_{2d} symmetry are described as

$$E(d_{z^2}) = e_\sigma(3\cos^2\theta - 1)^2 + 3e_{\pi\parallel}\sin^2 2\theta - 2\sqrt{3}e_{\pi\sigma\parallel}\sin 2\theta\,(3\cos^2\theta - 1)$$

$$E(d_{x^2-y^2}) = 4e_\pi \sin^2\theta$$

$$E(d_{xy}) = 3e_\sigma \sin^4\theta + e_{\pi\parallel}\sin^2 2\theta + 2\sqrt{3}e_{\pi\sigma\parallel}\sin^2\theta\sin 2\theta$$

$$E(d_{yz,zx}) = {}^3/_2 e_\sigma \sin^2 2\theta + 2e_\pi\cos^2\theta + 2e_{\pi\parallel}\cos^2 2\theta + \sqrt{3}e_{\pi\sigma\parallel}\sin 4\theta \quad (3)$$

where θ is the half of the S–M–S′ angle containing the z axis, and $2\theta = 96.3°$ for this complex.[14] e_π represents the effect of the sulfur π-bonding orbital. e_σ, $e_{\pi\sigma\parallel}$, and $e_{\pi\parallel}$ represent the σ-bonding effect, where the latter two are extra parameters introduced to take into account the off-axis component due to the misdirected valency.[17] These two parameters will vanish if the direction of the sulfur σ-bonding orbital coincides with the M–S bond direction. In applying the AOM to our complex, however, we should reduce the number of the parameters since four parameters are more than required for a complete description of a D_{2d} ligand field. In order to do this, we used the plausible relation $e_{\pi\sigma\parallel}{}^2 = e_\sigma e_{\pi\parallel}$, which follows from eqs 3 and 5 in ref 17. Then the substitution of the above d-orbital energies into eqs 3 yields $e_\sigma = 3700$, $e_\pi = 1870$, $e_{\pi\sigma\parallel} = 810$, and $e_{\pi\parallel} = 180$ cm^{-1}.

The AOM calculation unequivocally shows that a strong π interaction is incorporated in the cobalt(II)–thiolate sulfur bonding ($e_\pi/e_\sigma = 0.51$). Evidently, under the D_{2d} geometry, the sulfur π orbitals will overlap mostly with $d_{x^2-y^2}$ and to a lesser extent with $d_{yz,zx}$ whereas no overlaps will occur with d_{z^2} or d_{xy} (Figure 9). Therefore the energy order of $d_{z^2} < d_{x^2-y^2} < d_{xy} < d_{yz,zx}$ with a large e-orbital splitting is expected. This splitting pattern is exactly what we have obtained. Another notable conclusion drawn from the AOM calculation is that the misdirection of the σ bonding is not a very important factor in the Co^{II} complex. However, it should be noted that this does not mean that the concept of

(28) In the final stage of the fitting, we attempted varying Δ_z as well as the other parameters. The fitting, however, resulted in an absurd value of $\Delta_z = 0$, though this may be another piece of evidence for the extreme low energy of the $^4A_2 \rightarrow {}^4T_2$ transition. Since the other parameter values resulting from this fitting are practically identical to the values obtained using $\Delta_z = 1000$ cm^{-1}, we do not vary Δ_z in the fittings described in the text.

(29) The polarization properties of the spin-forbidden transitions depend on the spin state of the ground state. For the present case, only the transitions from the lower Krammers doublet ($S_z = \pm^3/_2$) will appear. The transition $|^4A_2;\ S_z = \pm^3/_2\rangle \rightarrow |^2\Gamma;\ S_z = \pm^1/_2, \gamma\rangle$ will be x,y polarized for $\Gamma\gamma = A_1$, $E\theta$, $E\epsilon$, $T_1{}^z$, and $T_2{}^z$, and z polarized for $\Gamma\gamma = T_1{}^{x,y}$, $T_2{}^{x,y}$ according to the spin–orbit mediated intensity-borrowing machanism.

(30) Examples of the application of AOM to high-spin cobalt(II) complexes: (a) Horrocks, W. D., Jr.; Burlone, D. A. *J. Am. Chem. Soc.* **1976**, *98*, 6512–6516. (b) Bencini, A.; Benelli, C.; Gatteschi, D.; Zanchini, C. *Inorg. Chem.* **1979**, *18*, 2137–2140. (c) Bencini, A.; Benelli, C.; Gatteschi, D.; Zanchini, C. *Inorg. Chem.* **1979**, *18*, 2526–2528. (d) Banci, L.; Benelli, C.; Gatteschi, D.; Mani, F. *Inorg. Chem.* **1982**, *21*, 1133–1136.

misdirected valency is invalid. Inspection of eq 3 shows that the off-axis σ interaction *does* contribute to the d-orbital splitting, reducing the separation between d_{xy} and $d_{yz,zx}$. Therefore, the obtained δ value is smaller than expected for no off-axis σ interaction.

Properties of Iron(II)- and Iron(III)-Thiolate Bondings. The analogous Fe^{II} complex $(Ph_4P)_2[Fe(SPh)_4]$ is well-known to be a successful synthetic model of the active site of reduced rubredoxin. The coordination geometries of the Fe^{II} complex[14] and the rubredoxin active site[15] are similar to that of the Co^{II} complex in that the S-Fe-S-C torsion angles are ca. 180°. Although the overall d-orbital splittings for the Fe^{II} ions are not known, it is known that the ground d orbitals are d_{z^2} well separated from $d_{x^2-y^2}$ for both.[14,18] This splitting pattern is identical to that of the Co^{II} complex and suggests a substantial π interaction between the Fe^{II} ions and the thiolate sulfurs. The separations between d_{z^2} and $d_{x^2-y^2}$ are, however, remarkably reduced compared with the separation in the Co^{II} complex (μ = 4140 cm^{-1}): $\mu \geq 1000$[14] and $\approx$850 cm^{-1} [18] were estimated for the Fe^{II} model complex and reduced rubredoxin, respectively. (Although the μ value of the model complex is not known well, the value will not be very different from that of reduced rubredoxin.) The relatively small μ values suggest a weaker nature of the Fe^{II}-S π interaction.

The occurrence of weaker π interaction in iron(II)-sulfur bonding can also be evidenced by the recent spectroscopic study of $(Et_4N)_2[Fe(SC_6H_4\text{-}2\text{-}Ph)_4]$.[10] It was reported that this complex has a (strict) S_4 geometry with the S-Fe-S-C torsion angles being 47.6°, and hence the four π-bonding orbitals are directed to cancel with one another's effects on the e- and t_2-orbital splittings. We add to this that the π interaction can affect the splittings nevertheless by allowing a mixing between $d_{x^2-y^2}$ and d_{xy} (both d orbitals belong to the same representation B under S_4 symmetry). Therefore, if the π interaction were enough strong, the d-orbital splitting pattern would be $d_{x^2-y^2} < d_{z^2} < d_{yz,zx} < d_{xy}$. However the actual t_2-orbital splitting is such that d_{xy} is situated lower than $d_{yz,zx}$. This indicates that the π interaction competes with the off-axis σ interaction in the iron(II)-thiolate bonding.

The d-orbital splitting in an iron(III)-thiolate complex, $(Et_4N)[Fe(SC_6HMe_4)_4]$, was recently examined in detail.[8,9] In this complex, the S'-M-S-C torsion angles are all ca. 90° (S_4 symmetry).[31] Hence the d-orbital splitting pattern expected for strong π interaction is $d_{x^2-y^2} < d_{z^2} < d_{yz,zx} < d_{xy}$. However the actual splitting pattern is $d_{z^2} < d_{x^2-y^2} < d_{xy} < d_{yz,zx}$, and both e- and t_2-orbital splitting patterns are opposite to the expected ones. Therefore the π interaction between iron(III) and thiolate sulfur must be weak or even negligible as reported previously.[9]

In all likelihood, the findings about the cobalt(II)-thiolate bonding are easily understandable in the framework of the usual metal-ligand bonding scheme. Moreover, they compare well with previous molecular-orbital calculations,[6,7] though the calculations concerned iron thiolates. Thus the very weak π interaction for iron(III)-thiolate bonding is instead perplexing. The reason for the discrepancy between the theoretical and experimental results on the iron(III)-thiolate bonding is not known and is left for a future study.

Summary

The single-crystal ESR and susceptibility results have established significantly large ZFS and highly anisotropic g values in the cobalt(II)-thiolate complex. It is concluded that these magnetic properties arise from the combination of the D_{2d}-type thiolate coordination and the strong π interaction between cobalt(II) and thiolate sulfur. The finding of the strong π interaction is especially exciting. This contrasts cobalt(II)-thiolate bonding with iron(II)-thiolate bonding, where the π interaction is not very strong, and with iron(III)-thiolate bonding, where the π interaction is very weak. The findings presented here and elsewhere[3-5,8-10] can be summarized as the following series of metal ions arranged according to their ability to form π bonds with thiolate sulfur:

$$Fe^{III} < Fe^{II} < Co^{II} \sim Cu^{II}$$

Furthermore, the concept of misdirected valency seems to become more relevant in the reversed order.

Acknowledgment. We thank Dr. Hideki Masuda (Institute for Molecular Science, Okazaki, Japan) for the X-ray diffraction measurements. This work was partially supported by a Grant-in-Aid for Scientific Research from the Ministry of Education, Science and Culture, Japan.

Registry No. $(Ph_4P)_2[Co^{II}(SPh)_4]$, 57763-37-8.

(31) Millar, M.; Lee, J. F.; Koch, S. A.; Fikar, R. *Inorg. Chem.* **1982**, *21*, 4105-4106.

Contribution from the Inorganic Chemistry Laboratory, University of Oxford, South Parks Road, Oxford OX1 3QR, U.K.

Applications of Two-Photon Spectroscopy to Inorganic Compounds. 2. Spectrum and Electronic Structure of $CsUO_2(NO_3)_3$

Trevor J. Barker, Robert G. Denning,* and Jonathan R. G. Thorne

Received October 2, 1991

The low-temperature two-photon absorption spectrum of a single crystal of $CsUO_2(NO_3)_3$ is reported. The spectrum is much simpler than the single-photon absorption; together they locate nine excited electronic states. The symmetry of these states is determined, and their accurate location enables an assignment of excited-state vibrational frequencies. Only the frequencies of the uranyl cation modes are significantly modified compared to the ground state. With this data set we have refined our model of the excited-state configurations and the perturbation of the equatorial field. The results confirm that the electronic structural model of the uranyl core is transferable, with only minor modifications, between the tetragonal field of four chloride ions in $Cs_2UO_2Cl_4$ and the trigonal field of the three nitrate ions in $CsUO_2(NO_3)_3$.

Introduction

The single-photon electronic spectra of most uranyl compounds are extraordinarily complex. In part 1 of this series[1] we showed that the electronic excited states of $Cs_2UO_2Cl_4$ could be located much more readily using two-photon absorption spectroscopy (TPA) than by the familiar one-photon absorption spectroscopy (OPA). $Cs_2UO_2Cl_4$ crystallizes in a centrosymmetric space group, and as a result, the two experiments are largely complementary. TPA only enables transitions to the parity-conserving excited states and displays mainly the pure electronic transitions and totally symmetric progressions associated with them, while OPA shows the parity-changing transitions, which are exclusively induced by

(1) Barker, T. J.; Denning, R. G.; Thorne, J. R. G. *Inorg. Chem.* **1987**, *26*, 1721.

0020-1669/92/1331-1344$03.00/0